JGR Biogeosciences

METHOD
10.1029/2024JG008401

A Coupled O_2-CO_2 Model for Joint Estimation of Stream Metabolism, O-C Stoichiometry, and Inorganic Carbon Fluxes

Jacob S. Diamond[1] and **E. Bertuzzo**[1]

[1]Department of Environmental Sciences, Informatics and Statistics, University of Venice Ca' Foscari, Venice, Italy

Key Points:

- Model reproduces O_2-CO_2 dynamics in stream water
- Stream CO_2 outgassing is partitioned between internal and external sources
- Estimated O-C stoichiometry is different from unity

Supporting Information:

Supporting Information may be found in the online version of this article.

Correspondence to:

E. Bertuzzo,
enrico.bertuzzo@unive.it

Citation:

Diamond, J. S., & Bertuzzo, E. (2025). A coupled O_2-CO_2 model for joint estimation of stream metabolism, O-C stoichiometry, and inorganic carbon fluxes. *Journal of Geophysical Research: Biogeosciences*, *130*, e2024JG008401. https://doi.org/10.1029/2024JG008401

Received 6 AUG 2024
Accepted 21 MAR 2025

Author Contributions:

Conceptualization: Jacob S. Diamond, E. Bertuzzo
Methodology: Jacob S. Diamond, E. Bertuzzo
Software: Jacob S. Diamond, E. Bertuzzo
Supervision: E. Bertuzzo
Visualization: Jacob S. Diamond, E. Bertuzzo
Writing – original draft: Jacob S. Diamond, E. Bertuzzo
Writing – review & editing: Jacob S. Diamond, E. Bertuzzo

Abstract We determine where stream carbon dioxide (CO_2) comes from by developing a model for the joint estimation of stream metabolism, oxygen-carbon (O-C) stoichiometry, and fluxes of dissolved inorganic carbon (DIC), based on observations of stream oxygen (O_2) and CO_2 concentrations. The model is based on a stream reach mass balance of O_2, DIC, and total alkalinity, and it accounts for the carbonate system and the contribution of lateral flow. O_2 and DIC mass balances are coupled through stoichiometric coefficients for photosynthesis and combined autotrophic and heterotrophic respiration. Under the assumption of constant alkalinity and circumneutral pH, the model simplifies and includes 8 parameters, which are estimated through a Bayesian hierarchical framework. The model accurately reproduced time series of O_2 and CO_2 from three diverse sites across size and carbonate chemistry gradients. Results allow partitioning of the stream DIC budget, and thus the source of stream CO_2 outgassing, into internal (in-stream net ecosystem production) and external (lateral input of terrestrial DIC and atmospheric input) contributions. We observed that the estimated stoichiometric coefficients were typically different from 1—contrary to typical assumptions—leading to divergent estimates of stream CO_2 sources depending on the measurement (i.e., O_2 vs. C). Parameter posterior distributions revealed the source of parameter uncertainty and the equifinality of some processes in reproducing stream CO_2 dynamics, suggesting targeted variables to further investigate in order to better constrain stream C balance. The proposed model is a useful tool for incorporating the rapidly growing stream CO_2 data sets into our understanding of terrestrial-aquatic C linkages.

Plain Language Summary The metabolism of streams and rivers is defined by two key processes: production, during which autotrophic organisms synthesize organic carbon by absorbing carbon dioxide (CO_2) and releasing oxygen (O_2), and respiration, where organic carbon is broken down, consuming O_2 and releasing CO_2 and energy. Because production occurs only during daylight hours, when light is available for photosynthesis, this leads to diel fluctuations in the concentrations of O_2 and CO_2 in stream water. In this study, we developed a model that leverages joint observations of O_2 and CO_2 to estimate not only stream metabolism but also the ratio of carbon to oxygen usage and the lateral fluxes of inorganic carbon leaking from terrestrial to stream ecosystems. The results address two emerging issues in freshwater biogeosciences: accurately estimating CO_2 emissions and closing the carbon budget at catchment, regional, and global scales.

1. Introduction

There is an unexplained gap (ca. 1.5 Pg-C y^{-1}) between estimates of terrestrial carbon (C) lateral export to receiving waters and resulting freshwater CO_2 emissions (Battin et al., 2009; Kirk & Cohen, 2023; Regnier et al., 2013). The ultimate source of observed freshwater carbon dioxide (CO_2) emissions therefore remains an important uncertainty in our understanding of the connection between terrestrial and freshwater ecosystems and ultimately the global C cycle (Battin et al., 2023; Bernhardt et al., 2022). Streams and rivers represent the largest share of freshwater CO_2 emissions (Drake et al., 2018), driving research focus to their dynamics and raising the question of whether, and in what proportion, their observed CO_2 is (a) produced from in-stream respiration of organic carbon or (b) delivered directly to streams from terrestrial soils as dissolved inorganic carbon (DIC). Resulting from this interest are an increasing number of subdaily resolution CO_2 data sets (https://data.stream-pulse.org, Appling, Read, et al. (2018)) that have the potential to reveal the relative magnitudes of so-called internal versus external C sources (Bernal et al., 2022; Hotchkiss et al., 2015; Kirk & Cohen, 2023).

A long history of metabolism estimates derived from oxygen (O_2) concentration time series informs our understanding of stream ecosystem respiration (ER) and gross primary production (GPP) (Bernhardt et al., 2022;

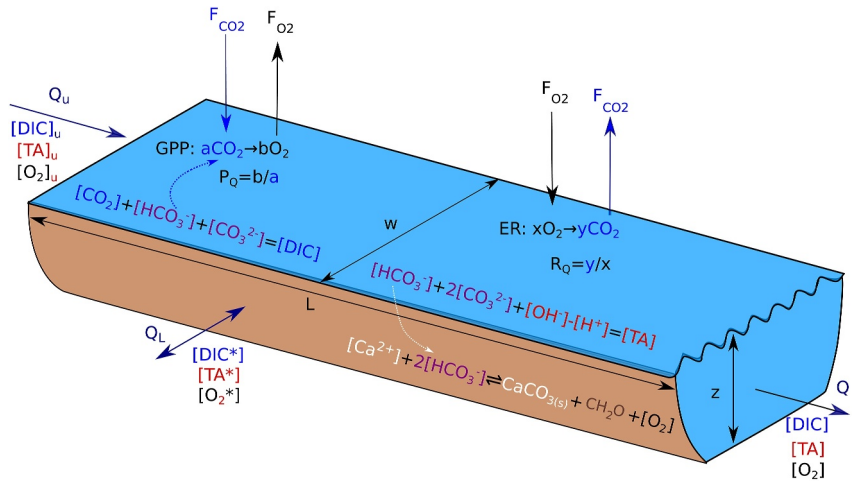

Figure 1. Conceptual setup of the model domain. State variables and their component chemical species are shown in like colors DIC, blue; TA, red; and O_2, black. Shared component species among TA and DIC are shown in purple. Also shown are relevant fluxes including GPP, ER (and their DIC-O_2 coupling coefficients), and biogenic calcite precipitation (white), which removes TA in addition to DIC. A blue dotted line from HCO_3^- to CO_2 indicates that the full model does not distinguish between these species for GPP uptake of DIC, as autotrophic uptake of both HCO_3 and CO_2 induces identical changes in pH, and neither pathway affects TA.

Mulholland et al., 2001; Odum, 1956). Indeed, hundreds of stream reaches across nearly 70 years have employed a O_2 mass balance method to simultaneously determine GPP, ER, and atmospheric gas exchange (Demars et al., 2015). By contrast, direct estimates of external CO_2 transport to streams are far more limited as they require measurements of both lateral flow and CO_2 concentration in groundwater (Kirk & Cohen, 2023). Thus, of the two potential stream CO_2 sources, internal generation via heterotrophic net ecosystem production (NEP = GPP–ER, ER > GPP) is the most constrained (Hotchkiss et al., 2015), leading to estimation of external sources by difference. There is an untapped potential in stream CO_2 time series to directly estimate both sources and therefore begin to close the C gap between terrestrial and freshwater ecosystems.

Inherent to the O_2 balance method is an assumption of a fixed ratio (1:1 or sometimes 1.2:1) between O_2 and C based on the production and consumption of organic carbon by photosynthesis and respiration, respectively (Aho et al., 2021a; Hotchkiss et al., 2015). Contemporary evidence suggests that this stoichiometry—referred to as the photosynthetic (mol O_2/mol CO_2, P_Q) and respiratory (mol CO_2/mol O_2, R_Q) quotients—varies widely depending on environmental conditions (Berggren et al., 2012; Trentman et al., 2023). This implies that our understanding of C fluxes based on decades of O_2 modeling may be biased, potentially explaining a substantial proportion of variation in internal CO_2 production. Thus, there is an obvious need to couple O_2 and CO_2 dynamics to constrain uncertainty in these key stoichiometric parameters.

We developed a reach-scale river model of subdaily CO_2 and O_2 dynamics based on mass balance of O_2, DIC, and total alkalinity, and used it to jointly estimate metabolic fluxes (GPP and ER), the stoichiometric quotients (P_Q and R_Q), and the fluxes of DIC, and, as a result, the magnitude of external and internal sources of CO_2 outgassing. We hypothesized that the model would not generate substantially different values for GPP, ER, or gas exchange compared to O_2 mass balance approaches as these are relatively robust. However, we expected that the model would improve understanding of P_Q, R_Q, and lateral DIC flux given that lateral discharge was constrained.

2. Methods

2.1. Model Equations

We consider a stream reach of length L [m], average width w [m], and time varying average depth $z(t)$ [m], which stores a water volume $V(t) = w\,z(t)L$ [m^3]. The reach receives inflow from upstream, $Q_u(t)$ [$m^3\ d^{-1}$], and laterally, $Q_L(t)$, and discharges streamflow to the downstream reach, $Q(t)$ (Figure 1). Note that in the case of a losing stream, $Q_L(t)$ is negative and represents a flow output.

The model equations are derived from the coupled reach-scale mass balance of water and three quantities that are conservative under mixing: oxygen (O_2), dissolved inorganic carbon (DIC), and total alkalinity (TA). Note that mass balance of water translates into a volume balance when water is approximated as an incompressible fluid. The mass balance is driven by hydrologic flows, GPP and ER, gas exchange at the water-air interface (F), possible calcite precipitation/dissolution, and advection and mixing in the stream water. The model assumes that the reach is a well-mixed reactor, and thus, the mass balances translate into the following set of ordinary differential equations:

$$\frac{dV(t)}{dt} = Q_u(t) + Q_L(t) - Q(t) \tag{1}$$

$$\frac{dM_{O_2}(t)}{dt} = Q_u(t)O_{2,u}(t) + Q_L(t)O_2^*(t) - Q(t)O_2(t) + L \cdot w[\mathrm{GPP}(t) - \mathrm{ER}(t) + F_{O_2}(t)] \tag{2}$$

$$\begin{aligned}\frac{dM_{\mathrm{DIC}}(t)}{dt} = {} & Q_u(t)\mathrm{DIC}_u(t) + Q_L(t)\mathrm{DIC}^*(t) - Q(t)\mathrm{DIC}(t) \\ & + L \cdot w\left[-\frac{\mathrm{GPP}(t)}{P_Q(t)} + R_Q(t)\mathrm{ER}(t) + F_{CO_2}(t) + g_{\mathrm{DIC}}(t)\right]\end{aligned} \tag{3}$$

$$\frac{dM_{\mathrm{TA}}(t)}{dt} = Q_u(t)\mathrm{TA}_u(t) + Q_L(t)\mathrm{TA}^*(t) - Q(t)\mathrm{TA}(t) + L \cdot w \cdot g_{\mathrm{TA}}(t) \tag{4}$$

where $M_{O_2}(t)$, $M_{\mathrm{DIC}}(t)$, and $M_{\mathrm{TA}}(t)$ represent mass (in [mol] and [Eq] for TA) of the respective quantities, while $O_2(t)$, DIC(t), and TA(t) the corresponding well-mixed volumetric concentrations [mol m^{-3}]. Concentrations with subscripts u refer to the concentrations in the upstream inflow. Concentrations with an asterisk (*) are equal to the concentration of lateral flow when $Q_L(t) > 0$, and are equal to the stream water concentration when $Q_L(t) < 0$ (losing conditions). The bracketed terms in the right-hand side of Equations 2–4 represent fluxes per unit of benthic stream area [mol m^{-2} d^{-1}] that affect the state variable mass balance. They are GPP(t), ER(t), $F_{O_2}(t)$, and $F_{CO_2}(t)$. We note that because we account for the effect of GPP on DIC mass balance, and not on CO_2, this setup allows modeling the direct autotrophic HCO_3^- uptake, which is observed in CO_2 limited ecosystems and in streams with high TA (Aho et al., 2021a; Maberly & Gontero, 2017). For completeness, we also indicate flux terms, $g_{\mathrm{DIC}}(t)$ and $g_{\mathrm{TA}}(t)$, for additional biological and physical processes, such as calcification, which reduces both DIC and TA (Wolf-Gladrow et al., 2007), although these processes are not further considered in the remainder of the paper. P_Q and R_Q represent the photosynthetic (i.e., the molar ratio between O_2 and DIC for primary production) and the respiratory (i.e., the molar ratio between CO_2 and O_2 for ecosystem respiration) quotients, which couple the O_2 and DIC mass balances.

The model equations can be simplified by assuming that the upstream reach shares similar conditions with the focus reach, an inherent assumption in single-station O_2 analyses (Hall & Hotchkiss, 2017). Specifically, this assumption implies a stream section upstream that (a) shares similar conditions with the focus reach and that (b) is sufficiently long to be unaffected by initial conditions (see the detailed derivation in Reichert et al., 2009). Using this assumption, the resulting model equations read (see detailed derivation in Supporting Information S1) as the following:

$$\frac{dO_2(t)}{dt} = \frac{\mathrm{GPP}(t)}{z(t)} - \frac{\mathrm{ER}(t)}{z(t)} + \frac{q_L(t)}{z(t)}\left[O_2^*(t) - O_2(t)\right] + K_{O_2}(t)[O_{2,\mathrm{sat}}(t) - O_2(t)] \tag{5}$$

$$\begin{aligned}\frac{d\mathrm{DIC}(t)}{dt} = {} & \frac{g_{\mathrm{DIC}}(t)}{z(t)} - \frac{\mathrm{GPP}(t)}{z(t)P_Q(t)} + R_Q\frac{\mathrm{ER}(t)}{z(t)} + \frac{q_L(t)}{z(t)}[\mathrm{DIC}^*(t) - \mathrm{DIC}(t)] \\ & + K_{CO_2}(t)[CO_{2,\mathrm{sat}}(t) - CO_2(t)]\end{aligned} \tag{6}$$

$$\frac{d\mathrm{TA}(t)}{dt} = \frac{g_{\mathrm{TA}}(t)}{z(t)} + \frac{q_L(t)}{z(t)}[\mathrm{TA}^*(t) - \mathrm{TA}(t)] \tag{7}$$

where $q_L(t) = Q_L(t)/(w \cdot L)$ represents the lateral discharge per unit of streambed area [m d^{-1}]. Stream-atmosphere gas exchange is modeled using Fick's Law with the atmospheric saturation concentration ($O_{2,sat}$ and $CO_{2,sat}$ [mol m^{-3}]) and the gas exchange rates (K_{O_2} and K_{CO_2} [d^{-1}]) (Wanninkhof et al., 2009). In the case of a losing reach, one has $DIC^*(t) = DIC(t)$, $O_2^*(t) = O_2(t)$, and $TA^*(t) = TA(t)$, and thus, the terms related to q_L are null, which implies that the lateral flow has, as expected, no effect on these variables.

The exchange flux of DIC with the atmosphere is a function of CO_2 concentration, invoking the need to calculate the water carbonate system. Equilibration of carbonate species occurs with a time scale (around minutes) shorter than the typical diel fluctuations of the quantities considered. Therefore, using the principle of timescale separation, we assume instantaneous equilibria among the carbonate species. At each time t, we calculate $CO_2(t)$ [mol m^{-3}] and pH(t) based on TA(t), DIC(t), and water temperature using a standard Newton-Raphson iterative scheme (Stumm & Morgan, 2012).

2.2. Simplified Model

Equations 5–7 account for TA variation and its effect on the carbonate system. This may be desired to incorporate carbonate dynamics (e.g., $HCO_3^- + H^+ \leftrightarrow CO_2 + H_2O$) or to quantify biophysical processes affecting TA ($g_{TA}(t)$, e.g., calcification). However, in many cases of practical interest, TA can be approximated as constant ($dTA/dt = 0$), simplifying calculations. In streams, such conditions typically require the following:

- Constant or baseflow discharge so that TA is in equilibrium with the lateral flow. Varying source activation under stormflow or hydrologically dynamic conditions likely induces temporal variation in TA.
- Negligible calcite dissolution and precipitation.

Additional considerations may be important depending on the model application that violate the constant TA assumption. For example, high catchment evapotranspiration may induce diel variation in alkalinity (an argument posited by Shangguan et al., 2021) with consequences for accurate modeling of the carbonate system. We note that direct HCO_3^- uptake by autotrophs under low CO_2 conditions does not affect TA (Maberly & Gontero, 2017).

Additional model simplification is achieved when CO_3^{2-} is negligible (e.g., pH < 8.5–9, depending on temperature), a common condition in many streams and rivers. Indeed, if one approximates total alkalinity in freshwater with the carbonate alkalinity $TA \approx [HCO_3^-] + 2[CO_3^{2-}]$, and $CO_3^{2-} \approx 0$, one has that $TA \approx [HCO_3^-] \approx$ constant. Therefore

$$\frac{dDIC}{dt} = \frac{dCO_2}{dt} + \frac{dHCO_3^-}{dt} + \frac{dCO_3^{2-}}{dt} = \frac{dCO_2}{dt} \tag{8}$$

Under these assumptions and approximations, Equations 5–7 simplify to:

$$\frac{dO_2(t)}{dt} = \frac{GPP(t)}{z(t)} - \frac{ER(t)}{z(t)} + \frac{q_L(t)}{z(t)}[O_2^*(t) - O_2(t)] + K_{O_2}(t)[O_{2,sat}(t) - O_2(t)] \tag{9}$$

$$\begin{aligned}\frac{dCO_2(t)}{dt} = &-\frac{GPP(t)}{z(t)P_Q(t)} + R_Q(t)\frac{ER(t)}{z(t)} + \frac{q_L(t)}{z(t)}[DIC^*(t) - HCO_3^- - CO_2(t)] \\ &+K_{CO_2}(t)[CO_{2,sat}(t) - CO_2(t)]\end{aligned} \tag{10}$$

where HCO_3^- is the stream water bicarbonate concentration, which is constant under the above assumptions. The advantage of the assumption of negligible CO_3^{2-} is that the ODE system reduces to the most common state variables of interest: O_2 and CO_2. Moreover, this model formulation eliminates the need to solve the carbonate equilibrium at each time step. This decreases model runtime, an important feature when performing Bayesian parameter estimation via Markov chain Monte Carlo.

2.3. Numerical Implementation

Equations 9 and 10 are integrated numerically with an Euler explicit scheme with a time step of 15 min. We checked the accuracy of the method by simulating the model with shorter time steps and comparing the results.

The temperature-dependent O_2 gas exchange rate is calculated from the parameter K_{600} (d^{-1}), the gas exchange rate at the Schmidt number 600 (i.e., the Schmidt number of CO_2 at 20°C in freshwater):

$$K_{O_2}(t) = K_{600}(t)\left(\frac{600}{Sc_{O_2}(T(t))}\right)^{0.5} \tag{11}$$

where $Sc_{O_2}(T(t))$ is the function relating the Schmidt number for O_2, Sc_{O_2}, to the water temperature $T(t)$ (Wanninkhof et al., 2009). K_{CO_2} is computed using Sc_{CO_2}, the Schmidt number for CO_2.

In the general application, the simplified model Equations 9 and 10 comprises 8 parameters, which need to be assigned or estimated (See Table 2). They are as follows: GPP, ER, q_L, $O_{2,L}$, DIC'_L, K_{600}, P_Q, and R_Q. $DIC'_L(t) = DIC_L(t) - HCO_3^-$ is a combined parameter used in the estimation.

As customary in estimation of stream metabolism, (e.g., Hall & Hotchkiss, 2017) GPP is assumed to be a linear function of light $L(t)$ according to

$$GPP(t) = GPP_d\frac{L(t)}{L_d} \tag{12}$$

where GPP_d and L_d are the mean of GPP and light values of day d, respectively. The units of $L(t)$ are immaterial because of the normalization by L_d. The environmental forcings needed to run the model are $L(t)$, $T(t)$, and $z(t)$.

Compared to typical applications of stream metabolism estimation based on diel O_2 observations, our model setup introduces two improvements. First, when observational error is assumed (see below), the simulation is run over several consecutive days while specifying only the initial conditions at the beginning of the simulation. Although setting separate initial conditions for each day is a valid approach—particularly when long time series are available or there are gaps in the data (see, e.g., Appling, Hall, et al., 2018)—using a single initial condition leverages the additional information of the continuity of O_2 and CO_2 time series across days. This ensures that there are no artificial step changes at midnight, reflecting the inherent smoothness of the processes. Second, parameters are assumed to change smoothly across days. Typical applications estimate separate parameter sets—such as mean daily ER, GPP, and K_{600}—for each day. While we adopt a similar approach, we also account for smooth day-to-day variations. Specifically, this is performed estimating the parameter values at noon of each day of the time series (e.g., ER_d, and $d = 1, \ldots, N_d$, where N_d is the number of days in the time series) and deriving the parameter value at each time (e.g., ER(t)) through linear interpolation of noon values. Thanks to these two improvements in the model setup the resulting simulated time series for O_2 and CO_2 are mathematical functions of class C^1: continuous and differentiable functions with continuous first derivatives.

2.4. Bayesian Parameter Estimation

Parameter estimation is performed in a Bayesian framework by sampling the parameter posterior distribution via a Markov chain Monte Carlo algorithm.

To test the model sensitivity to error structure, we employed two different error models: an observation error model and a process error model (for a detailed illustration of the two types of error in this context, the reader is referred to Appling, Hall, et al. (2018) and Song et al. (2016)). For the observation error model, the error, ϵ_{obs}, between the simulated and observed concentrations of O_2 and CO_2, is an independent, identically distributed normal variable with a mean of 0 and standard deviation σ; for example, $\epsilon_{O_2,obs}(t) = O_{2,mod}(t) - O_{2,obs}(t) = \mathcal{N}(0, \sigma_{O_2})$. For the process error model, or the one-step-ahead model, the equations are used to evolve the system from an observation at time t, used as initial condition, to an estimate at time $t + \Delta t$, and the error, for example, $\epsilon_{O_2,proc}$, is calculated at time $t + \Delta t$: $\epsilon_{O_2,proc}(t + \Delta t) = O_{2,mod}(t + \Delta t) - O_{2,obs}(t + \Delta t) = \mathcal{N}(0, \sigma_{O_2})$.

We additionally tested model sensitivity to parameterization by comparing the simplified eight-parameter model with two other formulations. The first is the "classical" O_2 mass balance model with three parameters (GPP, ER, and K_{600}). The second expands the classical model by introducing lateral discharge, and thus two additional parameters (q_L and $O_{2,L}$). The additional model formulations are only conditioned on error in O_2, and we compare GPP, ER, and K_{600} across the formulations. Finally, we assess the model sensitivity to the duration of the observed time series by repeating the estimation using half and one-quarter of the days in the data set.

We generally provide uninformative priors (uniform marginal distribution within a wide range) for parameters. When available and depending on the case study, informative priors are assigned to some parameters. In some other cases, priors are defined by hyperparameters, which follow hyperprior distributions in a hierarchical Bayesian framework. The detailed prior specification is reported after the three cases study are illustrated. Throughout the paper, results are reported as the median value and the 95-percentile range of the posterior distribution.

2.5. Case Studies

We searched the literature and data repositories for data sets containing jointly measured O_2 and CO_2 data, and we selected three suitable case studies, with varying hydrology and carbonate chemistries, to test the model (Table 1). We refer the readers to the original papers (Aho et al., 2021a; Kirk & Cohen, 2023) for additional information on each site, but note here that Union is a shallow, gravel-bed site on the Farmington River, Connecticut; Phelps is a small forested tributary to the Farmington River, located approximately 1 km upstream from a large reservoir; and SF2500 is a limestone-aquifer spring-fed river in Florida. From each site, we estimated model parameters using a time series with length varying from 8 to 13 days, chosen based on data quality and condition of baseflow. When light data were not available, we assumed light as proportional to the clear-sky solar radiation, which was calculated based on the hour of the day, day of year, latitude, and longitude (Thackston & Parker, 1971).

We estimated for each site lateral flow in order to provide informative priors for q_L and avoid model equifinality. To this end, we estimated q_L in one of two ways. (a) We differenced the discharge between the nearest (Q_1) and the closest upstream United States Geological Survey (USGS) discharge gage (Q_0). (b) We calculated the catchment area at the measurement site (A_1) and the catchment area for a site located approximately 1,000 m upstream (A_0). We then estimated the lateral discharge as $Q_1(1 - A_0/A_1)$ assuming the two sites have the same specific discharge. To estimate q_L from these quantities, we divided this discharge by the distance between sites and by the average stream width as estimated from Google Earth.

Table 2 details the prior specifications for all parameters and case studies. After some initial trials, we note a strong equifinality at the Union and Phelps sites between the gas exchange rate K_{600} and metabolic fluxes GPP and ER. This is a known and common issue in the metabolism estimation (Appling, Hall et al., 2018) where equally good fitting of O_2 (and CO_2 in this case) can be achieved suitably increasing, or decreasing, both K_{600} and metabolic fluxes. To overcome this issue, we provide for these two sites an informative prior centered around the K_{600} estimated from hydraulic geometry (Raymond et al., 2012, Equation 1 in Table 2).

Two additional pairs of parameters that are difficult to independently estimate are q_L and DIC'_L, and q_L and $O_{2,L}$, because their products appear in the model equations. For this reason, we use informative priors for q_L based on the estimates previously described. We further use a prior for $O_{2,L}$, which assumes lateral flow is between oxygen saturation and depletion. No further assumption is instead done for DIC'_L.

For parameters DIC'_L, P_Q, and R_Q, we do not specify prior information, but we implemented a hierarchical Bayesian framework in order to allow day-to-day variability while maintaining interday consistency. We use a different parameter for each day but impose that they all follow the same prior distribution defined by hyperparameters, which are included in the estimation. Uninformative hyperpriors are assumed except for the parameters controlling the mean of the prior distribution of P_Q and R_Q. For these parameters, the hyperprior specifies that the mean of the prior distributions of P_Q and R_Q fluctuates around 1, the theoretical value for glucose synthesis and respiration.

Using the prior specification described above for site SF2500, we obtained quite large day-to-day variations in the parameters K_{600}, R_Q, and DIC'_L, which seem unlikely given that the time series covers a period of almost constant baseflow discharge. To investigate if this is an identifiability issue, we estimated parameters in a simplified setup

Table 1
Site Characteristics for Combined O_2 and CO_2 Data Sets Over the Model Fitting Period

Site	Period	Q	q_L	z	pCO_2	pH	TA	Reference
Union	13-20/8/2019	4.2	0.09	0.4	928	7.6	0.57	(Aho et al., 2021b)
Phelps	10-20/8/2019	0.004	0.04	0.1	1,207	6.6	0.10	(Aho et al., 2021b)
SF2500	28/6–7/7/2019	33.7	0.57	1.7	6,520	6.7	2.0	(Kirk & Cohen, 2022)

Note. Q is mean stream discharge in $\left[m^3\ s^{-1}\right]$ and q_L; in $\left[m\ d^{-1}\right]$, z [m] is average cross-sectional water depth, mean pCO_2 in [μ atm], mean DIC, and TA in $\left[mol\ m^{-3}\right]$ and $\left[mEq\ m^{-3}\right]$. Lateral discharge was reported in the original data set for the site SF2500; it was estimated with the area method for the site Phleps, and with the discharge method for the site Union. For the latter, USGS gages 01188090, 01186000, and 01186500 were used. Average cross-sectional water depth was available in the original data set for the site SF2500, and was estimated via the hydraulic-stage discharge relationship for the other two sites (gage USGS 01187830 for Phelps and gage USGS 01188090 for Union).

and compared the results. Such setup (reported in Table 2) assumes a constant K_{600} and DIC'_L for the 13-day long time series.

2.6. Code Details and Availability

Codes to run the model and reproduce the results are available in the public repository (https://zenodo.org/doi/10.5281/zenodo.13193593) in two programming languages: MatLab and Stan compiled in R. MatLab formulation uses the $DREAM_{ZS}$ (Vrugt et al., 2009) implementation of the Markov chain Monte Carlo algorithm. We ran 1 million simulations subdivided in three chains and used the last 25% of the runs to sample the posterior. Chain

Table 2
Model Parameters, Associated Units, and Prior Distributions Assumed for the Three Case Studies

		Prior		
	Unit	Union	Phelps	SF2500
Parameter				
ER	$mol\ m^{-2}d^{-1}$	$\mathcal{U}(0,3)$	$\mathcal{U}(0,3)$	$\mathcal{U}(0,3)$
GPP	$mol\ m^{-2}d^{-1}$	$\mathcal{U}(0,3)$	$\mathcal{U}(0,3)$	$\mathcal{U}(0,3)$
K_{600}	d^{-1}	$\mathcal{N}(13,2)$	$\mathcal{N}(30,5)$	$\mathcal{U}(0,50)$
q_L	$m\ d^{-1}$	$\mathcal{N}(0.1,0.01)$	$\mathcal{N}(0.05,0.01)$	$\mathcal{N}(0.6,0.06)$
$O_{2,L}$	$mol\ m^{-3}$	$\mathcal{E}(0.05)$	$\mathcal{E}(0.05)$	$\mathcal{E}(0.05)$
DIC'_L	$mol\ m^{-3}$	$\mathcal{LN}(\mu_{\log(DIC'_L)},\sigma_{\log(DIC'_L)})$	$\mathcal{LN}(\mu_{\log(DIC'_L)},\sigma_{\log(DIC'_L)})$	$\mathcal{U}(0,3)$
P_Q	–	$\mathcal{LN}(\mu_{\log(P_Q)},\sigma_{\log(P_Q)})$	$\mathcal{LN}(\mu_{\log(P_Q)},\sigma_{\log(P_Q)})$	$\mathcal{LN}(\mu_{\log(P_Q)},\sigma_{\log(P_Q)})$
R_Q	–	$\mathcal{LN}(\mu_{\log(R_Q)},\sigma_{\log(R_Q)})$	$\mathcal{LN}(\mu_{\log(R_Q)},\sigma_{\log(R_Q)})$	$\mathcal{LN}(\mu_{\log(R_Q)},\sigma_{\log(R_Q)})$
σ_{O_2}	$mol\ m^{-3}$	$\mathcal{U}(0,0.1)$	$\mathcal{U}(0,0.1)$	$\mathcal{U}(0,0.1)$
σ_{CO_2}	$mol\ m^{-3}$	$\mathcal{U}(0,0.1)$	$\mathcal{U}(0,0.1)$	$\mathcal{U}(0,0.1)$
Hyperparameter				
$\mu_{\log(DIC'_L)}$	$\log(mol\ m^{-3})$	$\mathcal{U}(-5,5)$	$\mathcal{U}(-5,5)$	–
$\sigma_{\log(DIC'_L)}$	$\log(mol\ m^{-3})$	$\mathcal{U}(0,5)$	$\mathcal{U}(0,5)$	–
$\mu_{\log(P_Q)}$	–	$\mathcal{N}(0,0.2)$	$\mathcal{N}(0,0.2)$	$\mathcal{N}(0,0.2)$
$\sigma_{\log(P_Q)}$	–	$\mathcal{U}(0,0.3)$	$\mathcal{U}(0,0.3)$	$\mathcal{U}(0,0.3)$
$\mu_{\log(R_Q)}$	–	$\mathcal{N}(0,0.2)$	$\mathcal{N}(0,0.2)$	$\mathcal{N}(0,0.2)$
$\sigma_{\log(R_Q)}$	–	$\mathcal{U}(0,0.3)$	$\mathcal{U}(0,0.3)$	$\mathcal{U}(0,0.3)$

Note. $\mathcal{N}(\mu,\sigma)$ indicates a normal distribution with mean μ and standard deviation σ, $\mathcal{LN}(\mu,\sigma)$ a lognormal distribution where μ and σ are the mean and the standard deviation of the logarithm of the random variable, respectively, $\mathcal{E}(\mu)$ an exponential distribution with a mean μ, and $\mathcal{U}(lb,ub)$ a uniform distribution in the range $[ub,lb]$. Gray cells indicate where one parameter for each day of the time series has been estimated.

convergence was assessed via the Gelman and Rubin diagnostic. For the Union case study (8-day simulation at 15-min time step), 1 million simulations takes around 5 min in a standard laptop computer.

The STAN implementation uses a Hamiltonian Markov chain algorithm with adaptive no-U-turn sampling (*cmdstanr* package Stan Development Team (2023); Gabry et al. (2023)). For this approach, we used four parallel chains with 500 warm-up, or burn-in, samples and 2,000 posterior draws. For the Union case study, the sampling process takes about 80 s.

3. Results

The simplified model (Equations 9 and 10) was able to replicate the main features of the O_2 and CO_2 time series for the three case studies. We report the root mean square error (RMSE) between observed and simulated concentrations to provide an easily interpretable measure of goodness of fit: median $\mathrm{RMSE}_{O_2} = 0.0050$, 0.0028, 0.0087 mol O_2 m^{-3}, $\mathrm{RMSE}_{CO_2} = 0.0041$, 0.0020, and 0.0070 mol CO_2 m^{-3} for sites Union, Phelps, and SF2500, respectively (Figures 2–4). When the same prior setup used for sites Union and Phelps was used for SF2500, there were high day-to-day parameter variations, in particular for K_{600}, DIC'_L, and P_Q (Figure S4 in Supporting Information S1). We considered this unrealistic given that the time series covers a period of near-constant flow. The simplified setup produced instead more consistent results (Figure 4).

Both the observation error model and the process error model performed similarly and produced similar estimates (Figures S1–S3 in Supporting Information S1), although the process error model for SF2500 was less accurate than the observation error model. This is a well-known problem with process error models (Song et al., 2016), which fit changes in concentration accurately, but tend to perform poorly for actual concentration trajectories when continuous simulations are run. Process error models also tended to estimate lower metabolic rates than observation error models. Given the simpler model formulation and its generally better performance, we present the observation error model as the main results here.

The duration of the data time series did not significantly affect the results (Figures S17–S19 in Supporting Information S1). Estimates obtained from shorter periods showed good agreement with those based on the full data set. As expected, uncertainty increased with shorter time series, particularly for parameters with a hierarchical structure (e.g., DIC'_L, R_Q, and P_Q), where estimation relies on information aggregated across all days in the time series to determine the hyperparameters.

Model results allowed us to estimate the time series of input (ER, net lateral input, and atmospheric input) and output (GPP and outgassing) fluxes to the stream DIC balance, and from this, we partitioned the source of CO_2 outgassing for the whole simulated period (Figures 2–4). The lateral flow, when positive, constitutes an input to the DIC balance equal to $Q_L \mathrm{DIC}_L$. At the same time, positive lateral flow increases discharge and thus simultaneously increases net export of DIC: $(Q - Q_u)\,\mathrm{DIC}$ (the reader is reminded that under the model assumptions, $\mathrm{DIC}_u = \mathrm{DIC}$). We term the net effect of these two processes as net lateral DIC contribution (Figures 2–4). Mathematically, this corresponds to $q_L(\mathrm{DIC}'_L - CO_2)$ when expressed as flux per unit of streambed area.

We observed some collinearity in the parameter posterior samples (Figures S11–S13 in Supporting Information S1). As anticipated, ER, GPP, and K_{600} were highly correlated $(R^2 > 0.5)$ for sites Union and Phelps. We also observed correlation between R_Q and DIC'_L, in particular for sites Union and SF2500, as both parameters control the input of DIC. From a mathematical viewpoint, their contributions to the DIC balance is different and thus potentially identifiable. The input $\mathrm{ER} \cdot R_Q$ is almost constant during the day (assuming low interday variation of parameters), while the term $q_L(\mathrm{DIC}'_L - CO_2)$ is modulated by the daily fluctuations of stream CO_2. However, if $\mathrm{DIC}'_L \gg CO_2$, like in the estimated values for Union and SF2500, the contribution related to DIC'_L is also fairly constant during the day, and the two input terms related to R_Q and DIC'_L become difficult to separate, hence the observed equifinality. For site SF2500, which was strongly affected by the lateral flow q_L, we observed collinearity between ER and $O_{2,L}$. From a process viewpoint, this highlights how an increased respiration can be counterbalanced by an increased lateral oxygen concentration, leading to a similar O_2 trajectory. Finally, the model posterior sample for q_L tended to mirror the model prior, suggesting that CO_2 and O_2 data do not contain enough information to further constrain this parameter (Figures 2–4).

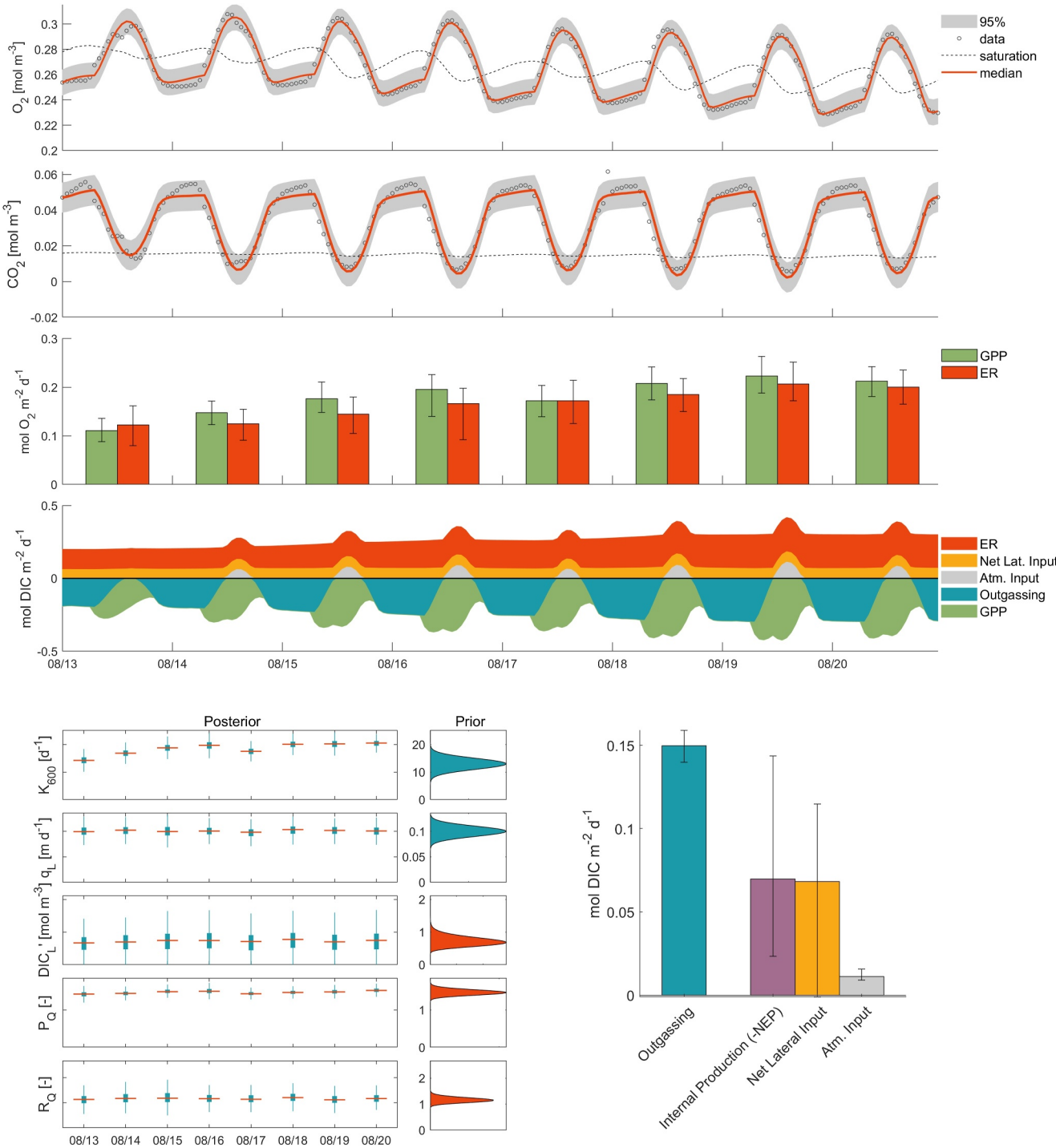

Figure 2. Model results for Farmington River at Unionville when observational error is assumed. From top to bottom: time series of O_2, CO_2, mean daily GPP and ER, and median fluxes controlling the DIC balance (positive (negative) values represent input (output) fluxes). The bottom left panel shows parameter marginal posterior distributions and associated prior. Red color indicates distributions whose shape is defined by estimated hyperparameters. Prior and posterior distributions of the remaining parameters (i.e., those that are constant during the simulation) are presented in the accompanying Figure S5 of Supporting Information S1. Bottom right: mean values over the analyzed period of outgassing flux and its estimated sources. Throughout the figure, results are displayed as the median and the 95 percentile-range of the posterior density except for the time series of DIC fluxes where only the median values are shown to facilitate the visualization.

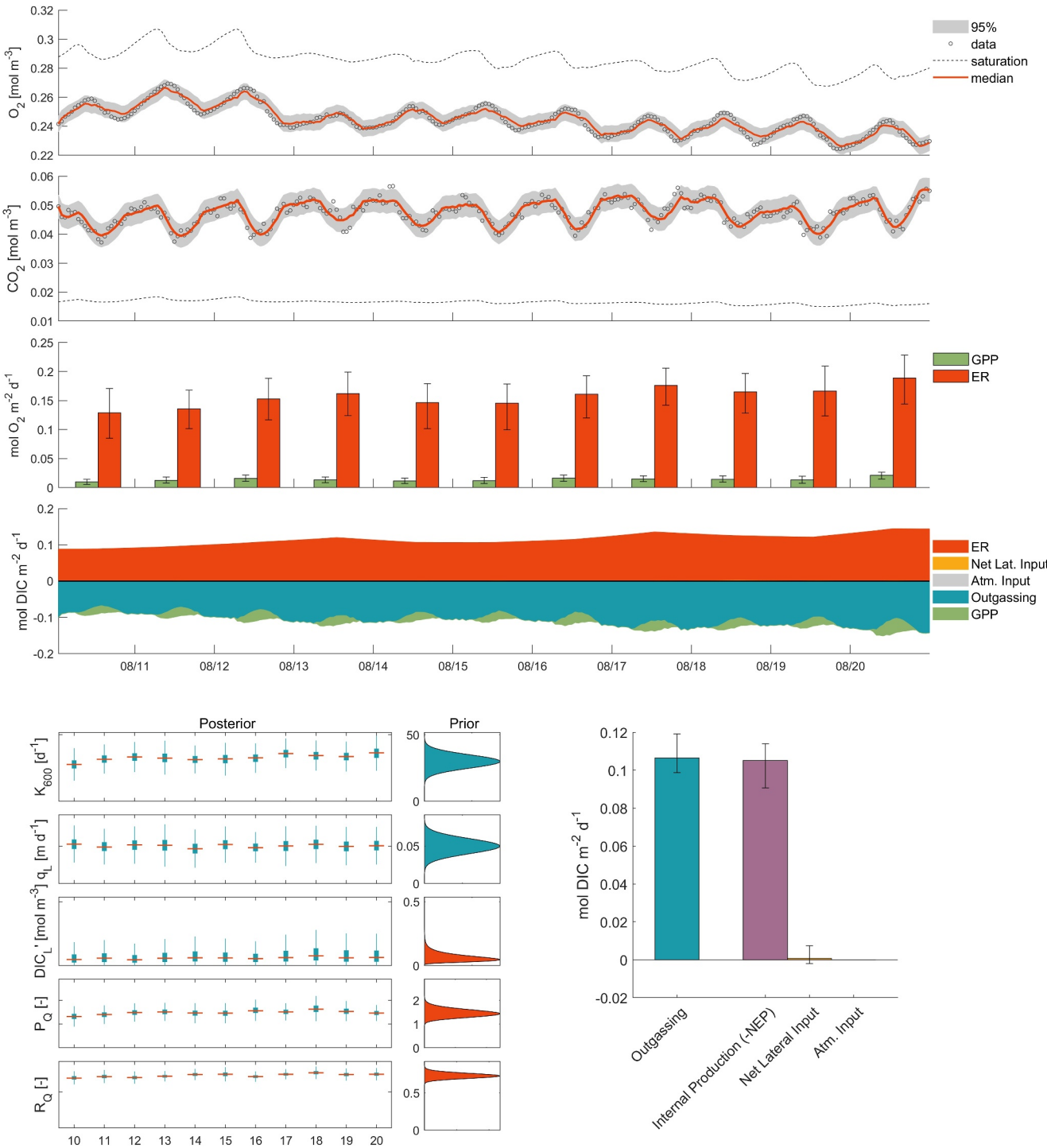

Figure 3. Results for the Phelps stream when observational error is assumed. Symbology as in Figure 2. Prior and posterior distributions of the remaining parameters (i.e., those that are constant during the simulation) are presented in the accompanying Figure S6 of Supporting Information S1.

3.1. Farmington River

The model was able to reproduce the finding of Aho et al. (2021a) that the Farmington River exhibited regular undersaturation of CO_2 relative to the atmosphere leading to diurnal atmospheric inputs (Figure 2). This undersaturation was not due to particularly large rates of GPP (ca. 0.1–0.2 mol O_2 m^{-2} d^{-1}).

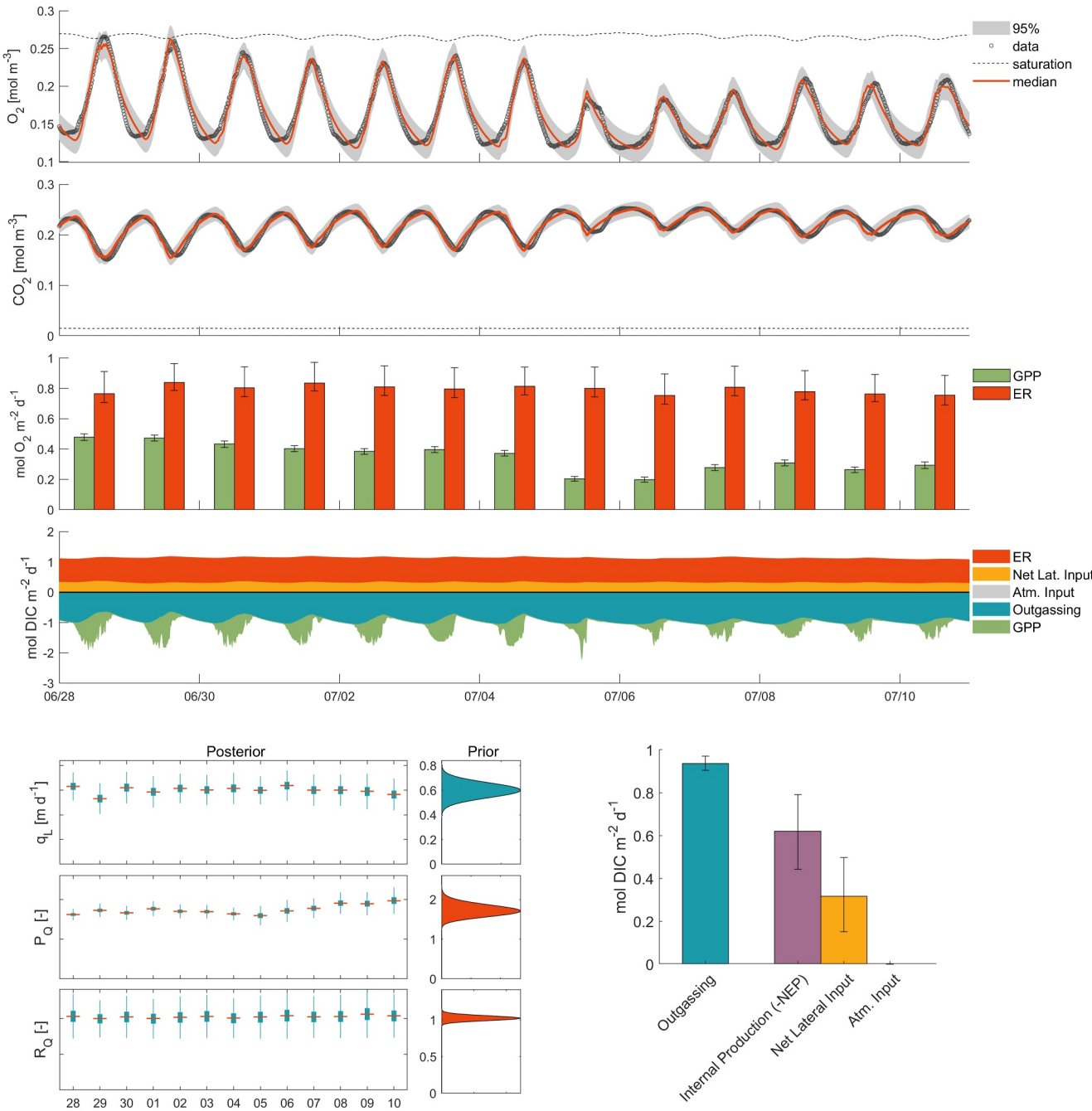

Figure 4. Results for Santa Fe River when observational error is assumed. Symbology as in Figure 2. Prior and posterior distributions of the remaining parameters (i.e., those that are constant during the simulation) are presented in the accompanying Figure S7 of Supporting Information S1.

Model results allow computing NEP in terms of both O_2 ($NEP_{O_2} = GPP - ER$) and C ($NEP_C = GPP/P_Q - ER \cdot R_Q$). The latter, with the opposite sign, represents the internal contribution to the DIC balance. For this site, we estimated a slightly autotrophic (i.e., positive NEP) system in terms of O_2 ($NEP_{O_2} = 0.014$ (−0.001, 0.0036) mol O_2 m^{-2} d^{-1}). However, an estimated median P_Q of 1.47 and R_Q of 1.14 (Figure 2) translated this into a net heterotrophic metabolic system from a C perspective ($NEP_C = -0.07$ (−0.14, −0.02) mol C m^{-2} d^{-1}). Nearly equal DIC was estimated to be delivered to the river from lateral sources as from internal production (Figure 2), but there was large uncertainty in this proportioning. Estimates of GPP and ER were not particularly uncertain; however, their median values were close and thus their difference amplified the

uncertainty. In turn, due to the mass balance constraint, the lateral input was also uncertain and this translated to a wide posterior distribution for the parameter DIC'_L.

We note some difference between the GPP estimated here (0.18 (0.17, 0.19) mol O_2 m^{-2} d^{-1}) and in the original study (0.40 ± 0.3 mol O_2 m^{-2} d^{-1}). As the estimated K_{600} is similar, and our estimates based only on O_2 data are consistent with the estimates of the complete model (Figure S14 in Supporting Information S1), we attribute this difference to the possible different values used for water depth z. We reconstructed a discharge rating curve based on USGS channel data, while the original study could have used field knowledge to derive values of the water stage more representative of the whole upstream reach. However, we stress that in Equations 9 and 10 water depth represents a scale parameter that converts metabolic rates from a volumetric to an areal basis, and it does not affect the emission partitioning and the estimation of the other parameters.

3.2. Phelps Stream

Model results for the Phelps stream indicated nearly all of CO_2 degassed to the atmosphere derived from internal production (Figure 3). Estimates of GPP (0.014 (0.07, 0.023) mol O_2 m^{-2} d^{-1}) were in line with those of the original study (0.015 ± 0.015 mol O_2 m^{-2} d^{-1}). Also for this site, we observed no differences in GPP, ER, or K_{600} among model formulations (Figure S15 in Supporting Information S1). We estimated a credible difference between $NEP_{O_2} = -0.14$ (−0.16, −0.11) mol O_2 m^{-2} d^{-1} and $NEP_C = -0.10$ (−0.11, –0.09) mol C m^{-2} d^{-1}. Such difference is due to the estimated value of $R_Q = 0.73$ (0.65, 0.80). P_Q was also different from 1 ($P_Q = 1.48$ (1.14, 1.91)), but this did not affect NEP_C as GPP is almost negligible compared to ER.

3.3. Santa Fe River

Compared to the other sites, the SF2500 fit was less accurate and tended to lag O_2 and CO_2 observations during the afternoon/early evening, and exhibited steeper changes around daily minima and maxima than were observed (Figure 4). SF2500 exhibited consistent heterotrophy despite higher rates of GPP (0.34 (0.33, 0.35) mol O_2 m^{-2} d^{-1}, Figure 4). Our estimates of O_2-based metabolism and K_{600} were closely aligned with those of the original authors (Kirk & Cohen, 2023). Estimated values of the photosynthetic quotient larger than unity (P_Q =1.72 (1.52, 2.07)) led to an increased heterothropy in terms of C compared to O_2: NEP_{O_2} = –0.45 (−0.58, −0.40) mol O_2 m^{-2} d^{-1}; NEP_C = –0.62 (−0.79, −0.44) mol C m^{-2} d^{-1}.

Differently from the other two case studies, we observed a sensitivity to model formulation, where "classical" O_2-based estimates of both ER and K_{600} decreased by 15% with inclusion of q_L and by another 15% using the complete model (Figure S16 in Supporting Information S1). It was only with the full model, however, that K_{600} aligned with the original study's direct measurements. As we provided no informative prior of K_{600} at this site (Table 2), this highlights that the full model takes advantage of the increased information contained in CO_2 time series to more accurately constrain parameter posteriors.

After providing relatively tight priors for q_L based on the measurements of the original study, the model converged on a DIC'_L of 0.74 (0.46, 1.05) mol m^{-3}. DIC'_L is a combined model parameter equal to $DIC_L - HCO_3^-$. To provide an approximate comparison with the original measurements of $CO_{2,L}$, we can further assume that alkalinity in the stream is in equilibrium with that of the lateral flow, which may be valid during baseflow conditions in this spring-fed river. Under the hypothesis of minimal CO_3^{2-}, this translates into $HCO_3^- = HCO_{3,L}^-$, and thus, $DIC'_L = CO_{2,L} + HCO_{3,L}^- - HCO_3^- = CO_{2,L}$ (see Equation 10). Thus, the lower bound of our estimate of lateral CO_2 is in line with the measured in situ concentration (riparian flow 0.44 mol CO_2 m^{-3}, and upland groundwater 0.30 mol CO_2 m^{-3}) in the original study. Although this comparison is approximate, it is remarkable that the model was able to estimate the magnitude of the lateral CO_2 concentration solely based on in-stream measurements of O_2 and CO_2. The greater C-based NEP contribution estimated here (the original study assumed $P_Q = 1$) could help explaining the fraction of CO_2 outgassing that was not attributed to any source in Kirk and Cohen (2023).

4. Discussion

The model presented here represents an improved source tracking for stream and river CO_2 compared to previous inference-by-difference methods. Taking advantage of the combined information from CO_2 and O_2 time series,

we were able to partition CO_2 provenance between lateral inputs and internal production and to quantify the uncertainty in these fluxes. Model results indicated that internal production of CO_2 via NEP was, although to different degrees, the dominant source of stream CO_2 across three diverse streams during growing season conditions. While the limited set of case studies analyzed does not allow general conclusions, the tools proposed will hopefully facilitate a more systematic and quantitative assessment of CO_2 budget in flowing waters.

We designed the model used here to be flexible for a variety of approaches and needs, including the ability to account for the entire carbonate system, possible calcification effects, and observation or process error structure, and to be conditioned on O_2 and/or CO_2 observations. An additional, but unexplored, capacity of the model is to condition on pH data, which under most conditions is analogous to conditioning on CO_2. Thus, for sites with only O_2 and pH measurements, the model may be equally useful, potentially opening its utility to a vast range of data sets, although estimations of TA are still required. One downside of this approach is that carbonate system calculations are required, thus increasing model runtime.

Lateral DIC inputs were one of the most uncertain fluxes in the results (Figures 2–4). We note that for the simplified model, the combined parameter, DIC'_L, is approximately equal to $CO_{2,L}$ if stream water alkalinity is in equilibrium with lateral flow; otherwise $HCO_{3,L}^-$, and $CO_{3,L}^{2-}$ if present, can be an additional, but unquantified source of DIC that can rapidly be converted into CO_2 within the stream. While the simplified model accounts for the total contribution of lateral DIC, the role played by the different components of the water carbonate system cannot be unraveled in the current formulation. A more complete picture could be achieved using the full model (Equations 5–7), but at the cost of the need to estimate TA_L. Alternatively, the need to solve the balance for TA may be avoided by using direct measurements, for example, with automated sensors (Shangguan et al., 2021), or with estimates derived from electrical conductivity.

The proposed model employs a "single station" approach, meaning it uses observed variables at a single cross-section to estimate representative quantities for the upstream reach, and the conditions for its applicability must be carefully evaluated. Typically, these conditions imply no major discontinuities or heterogeneities within a reach length of approximately $L_u \sim 3V/K$, where V is the average cross-sectional streamflow velocity, and K is the gas exchange rate. This distance represents the length a parcel of water travels before losing memory of perturbations and reequilibrating with the system (Reichert et al., 2009). Shangguan et al. (2024) analyze the applicability of single versus two-station approaches for CO_2/DIC measurements in the presence of carbonate buffering. Specifically, carbonate buffering can slow the reequilibration time for CO_2 compared to O_2, thereby increasing the length of the upstream reach that influences DIC dynamics at the sampled cross-section. This, in turn, can make the applicability of the single-station approach more challenging as O_2 and CO_2 integrate different stream lengths. The simplified model Equations 9 and 10 can provide further insights into this process. When the conditions for the applicability of the simplified model (negligible CO_3^{2-} and constant alkalinity) are met, the equations for O_2 and CO_2 share the same structure. As a result, the reequilibration times for the two gases are similar, apart from the small difference between K_{O_2} and K_{CO_2}. This occurs because when alkalinity is constant and mostly composed by HCO_3^-; variations in DIC are absorbed by variations in CO_2: $dDIC/dt = dCO_2/dt$. When such conditions are not met, $dDIC/dt \neq dCO_2/dt$, and this results in a slowdown of the DIC reequilibration time compared to O_2. As shown by Stets et al. (2017), this is more likely to occur at a high alkalinity, where CO_3^{2-} can contribute significantly. Under these conditions, it is necessary to use the complete model (Equations 5 and 6) to account for carbonate equilibria reactions. In such cases, the conditions of the upstream reach and the DIC reequilibration time must be carefully evaluated to assess the applicability of a single-station approach. To verify these conditions, the development of a one-dimensional model of coupled DIC and CO_2 mass balances can be helpful. If the conditions are not satisfied, a two-station approach is recommended.

It should be emphasized that our approach assumes a lack of upstream discontinuities (e.g., tributaries or hydraulic jumps) not only for O_2 (as is typical in stream metabolism studies) but also for DIC and TA. The above discussion regarding the conditions for the applicability of the presented model could be relevant to the Phelps case study. Although the general expectation for a small stream is that CO_2 is predominately sourced from lateral inflow (Hotchkiss et al., 2015), we found that Phelps CO_2 outgassing could be almost completely sourced by internal production. This is possibly due to the peculiarity of the site and modeling time frames chosen: Phelps was characterized by low rates of lateral inflow during the summer, but winter might reveal contrasting behavior. It is also worth noting that while we estimate an upstream reach length L_u of approximately 150–200 m, the stream

crosses a wetland area 500–600 m upstream of the sampling station. As we were unable to verify in the field whether this wetland introduces discontinuities that persist to the sampling location, the results for this site should be interpreted with additional caution.

Model equifinality, while hindering parameter identification, sheds light on the physical processes that can lead to the same O_2 and CO_2 signals, highlighting important measurement gaps for future research efforts. Indeed, the equifinality between DIC_L and R_Q, highlights how, in many cases of practical interest, O_2 and CO_2 time series alone may not contain enough information to constrain these parameters. This equifinality animates the growing need for direct measurements of R_Q under varying environmental conditions to better inform prior distributions. In general, equifinality and uncertainty could be alleviated providing more informative prior distributions. Constrained estimates of lateral discharge and groundwater CO_2 and DIC concentrations—and their variation with stream discharge—emerge as clear targets. Indeed, our efforts here highlight that q_L magnitude is a dominant control on model accuracy and thus accurate partitioning of CO_2 provenance, invoking the need for regional and global estimates of lateral discharge. Moreover, hierarchical pooling of, for example, K_{600} versus discharge could be implemented to overcome equifinality (Appling, Hall, et al., 2018). Still, despite best efforts to reduce uncertainty, model equifinality may be intractable at certain scales under the current modeling framework, for example, due to the inherent correlation between CO_2 and K_{600} (Rocher-Ros et al., 2019).

One of the important results of this work is the quantitative assessment of P_Q and R_Q, and their uncertainties. Despite only analyzing three sites, our results identify that P_Q and R_Q are rarely equal to 1. We note that while simple regressions of O_2–CO_2 can inform P_Q and R_Q (Aho et al., 2021a; Vachon et al., 2020), it remains difficult to parse P_Q from R_Q because (a) when estimating P_Q in daylight, the effect of both R_Q and P_Q are cooccurring, and (b) because R_Q in particular may be indistinguishable from signals deriving from variation in DIC_L, as evidenced by model equifinality. Finally, the simple physical differences in O_2 and CO_2 atmospheric gas exchange lead to regression slope magnitudes greater than 1 with increasingly greater magnitudes at higher temperatures, even when $P_Q = R_Q = 1$ (see example in Figure S20 in Supporting Information S1). Thus, while O_2–CO_2 regression can represent a useful tool for an initial assessment, its results should be interpreted with caution and bearing in mind the potential confounding factors outlined above. By contrast, the proposed model accounts for all of these processes and their associated uncertainty, and indicates that P_Q is commonly at least 1.2 during the growing season, and that R_Q varies between less than 1 and more than 1 depending on site conditions. Considering only the improved estimate of P_Q, our model implies that previous estimates of internal CO_2 production based on O_2 signals may be underestimated. If R_Q is also greater than 1, then O_2-based estimates are biased even lower. Thus, our results suggest that internal CO_2 production estimates based on O_2 metabolic estimates need to properly account for the inherent uncertainty in P_Q and R_Q.

As the cost and reliability of in situ CO_2 sensors improve, their deployment is expected to become as commonplace as O_2 sensors are today. Consequently, we need models to evaluate the data streams they generate. Our model addresses this need by providing a flexible framework to estimate key parameters of the carbonate-O_2 system in flowing waters. Of particular novelty is its ability to simultaneously estimate P_Q, R_Q, and lateral CO_2 or DIC inflow—parameters that are typically assumed (as in the case of P_Q or R_Q) or estimated by difference (as in the case of lateral DIC inflow). In the case studies presented, CO_2 concentrations were measured using different methods: at site SF2500, CO_2 was monitored with a sensor, whereas at Phelps and Union, it was measured using showerhead equilibrators, which are generally considered more accurate. Notably, we did not use prior information about CO_2 measurement errors. For future applications involving sensor-based measurements, characterizing sensor error and incorporating this information as a prior could help prevent overconfidence in the data. Moreover, the Bayesian approach detailed here provides a straightforward way to quantify uncertainty in key parameters and the resulting carbon and oxygen fluxes. Potentially tractable improvements to our approach include the incorporation of state space modeling (i.e., accounting for both observation and process errors, see Appling, Hall, et al. (2018)), reductions in computational time, and mitigation of model equifinality as discussed above.

Finally, we hope that this model motivates efforts to deconvolve stream CO_2 provenance at network scales. Initial efforts to do so may use a deterministic version of the model across reaches in synthetic stream networks (Carraro et al., 2020), where metabolism can be predicted across space and time (Diamond et al., 2021, 2023; Koenig et al., 2019; Mejia et al., 2019; Rodríguez-Castillo et al., 2019; Segatto et al., 2023). In such synthetic networks, it

will be necessary to develop network scaling functions for q_L (Kalbus et al., 2006; Leach et al., 2017). Additional needs will be network scaling functions for lateral DIC, TA, and CO_2 concentrations, which are currently poorly constrained. More care will also need to be given in the consideration of losing and gaining reaches and how best to incorporate spatial versus temporal changes in lateral inflow. The model presented here is an important step toward constraining terrestrial C leakage to freshwater systems, and to ultimately closing the linked terrestrial-aquatic carbon budget.

Data Availability Statement

Data and codes to run the model and reproduce the results are available in the public repository: https://zenodo.org/doi/10.5281/zenodo.13193593.

Acknowledgments
This research has been carried out within the PNRR research activities of the consortium iNEST (Interconnected North–East Innovation Ecosystem) funded by the European Union Next GenerationEU (Piano Nazionale di Ripresa e Resilienza (PNRR) Missione 4 Componente 2, Investimento 1.5 D.D. 1058 23/06/2022, ECS_00000043). This manuscript reflects only the authors' views and opinions; neither the European Union nor the European Commission can be considered responsible for them. Open access publishing facilitated by Universita Ca' Foscari, as part of the Wiley - CRUI-CARE agreement.

References

Aho, K. S., Hosen, J. D., Logozzo, L. A., McGillis, W. R., & Raymond, P. A. (2021a). Highest rates of gross primary productivity maintained despite CO_2 depletion in a temperate river network. *Limnology and Oceanography Letters*, *6*(4), 200–206. https://doi.org/10.1002/lol2.10195

Aho, K. S., Hosen, J. D., Logozzo, L. A., McGillis, W. R., & Raymond, P. A. (2021b). *Paired CO_2–O_2 measurements from streams and rivers ver 1*. Environmental Data Initiative. https://doi.org/10.6073/pasta/68cfcebdede8d3a671cd426a1252f255

Appling, A. P., Hall, R. O., Yackulic, C. B., & Arroita, M. (2018a). Overcoming equifinality: Leveraging long time series for stream metabolism estimation. *Journal of Geophysical Research: Biogeosciences*, *123*(2), 624–645. https://doi.org/10.1002/2017JG004140

Appling, A. P., Read, J. S., Winslow, L. A., Arroita, M., Bernhardt, E. S., Griffiths, N. A., et al. (2018b). The metabolic regimes of 356 rivers in the United States. *Scientific Data*, *5*(1), 1–14. https://doi.org/10.1038/sdata.2018.292

Battin, T. J., Lauerwald, R., Bernhardt, E. S., Bertuzzo, E., Gener, L. G., Hall, R. O., et al. (2023). River ecosystem metabolism and carbon biogeochemistry in a changing world. *Nature*, *613*(7944), 449–459. https://doi.org/10.1038/s41586-022-05500-8

Battin, T. J., Luyssaert, S., Kaplan, L. A., Aufdenkampe, A. K., Richter, A., & Tranvik, L. J. (2009). The boundless carbon cycle. *Nature Geoscience*, *2*(9), 598–600. https://doi.org/10.1038/ngeo618

Berggren, M., Lapierre, J.-F., & del Giorgio, P. A. (2012). Magnitude and regulation of bacterioplankton respiratory quotient across freshwater environmental gradients. *The ISME Journal*, *6*(5), 984–993. https://doi.org/10.1038/ismej.2011.157

Bernal, S., Cohen, M. J., Ledesma, J. L. J., Kirk, L., Martí, E., & Lupon, A. (2022). Stream metabolism sources a large fraction of carbon dioxide to the atmosphere in two hydrologically contrasting headwater streams. *Limnology & Oceanography*, *67*(12), 2621–2634. https://doi.org/10.1002/lno.12226

Bernhardt, E. S., Savoy, P., Vlah, M. J., Appling, A. P., Koenig, L. E., Hall, R. O., et al. (2022). Light and flow regimes regulate the metabolism of rivers. *Proceedings of the National Academy of Sciences*, *119*(8). https://doi.org/10.1073/pnas.2121976119

Carraro, L., Bertuzzo, E., Fronhofer, E. A., Furrer, R., Gounand, I., Rinaldo, A., & Altermatt, F. (2020). Generation and application of river network analogues for use in ecology and evolution. *Ecology and Evolution*, *10*(14), 7537–7550. https://doi.org/10.1002/ece3.6479

Demars, B. O. L., Thompson, J., & Manson, J. R. (2015). Stream metabolism and the open diel oxygen method: Principles, practice, and perspectives: Problems in stream metabolism studies. *Limnology and Oceanography: Methods*, *13*(7), 356–374. https://doi.org/10.1002/lom3.10030

Diamond, J. S., Moatar, F., Cohen, M. J., Poirel, A., Martinet, C., Maire, A., & Pinay, G. (2021). Metabolic regime shifts and ecosystem state changes are decoupled in a large river. *Limnology & Oceanography*, *67*(S1). https://doi.org/10.1002/lno.11789

Diamond, J. S., Pinay, G., Bernal, S., Cohen, M. J., Lewis, D., Lupon, A., et al. (2023). Light and hydrologic connectivity drive dissolved oxygen synchrony in stream networks. *Limnology & Oceanography*, *68*(2), 322–335. https://doi.org/10.1002/lno.12271

Drake, T. W., Raymond, P. A., & Spencer, R. G. (2018). Terrestrial carbon inputs to inland waters: A current synthesis of estimates and uncertainty. *Limnology and Oceanography Letters*, *3*(3), 132–142. https://doi.org/10.1002/lol2.10055

Gabry, J., Češnovar, R., Johnson, A., & Bronder, S. (2025). Cmdstanr: R interface to 'CmdStan'. R package version 0.9.0. Retrieved from https://mc-stan.org/cmdstanr/

Hall, R. O., & Hotchkiss, E. R. (2017). Stream metabolism. In F. R. Hauer & G. A. Lamberti (Eds.), *Methods in stream ecology* (3rd ed., Vol. 2, pp. 219–233). Academic Press. https://doi.org/10.1016/b978-0-12-813047-6.00012-7

Hotchkiss, E. R., Hall, R. O. Jr., Sponseller, R. A., Butman, D., Klaminder, J., Laudon, H., et al. (2015). Sources of and processes controlling CO_2 emissions change with the size of streams and rivers. *Nature Geoscience*, *8*(9), 696–699. https://doi.org/10.1038/ngeo2507

Kalbus, E., Reinstorf, F., & Schirmer, M. (2006). Measuring methods for groundwater-surface water interactions: A review. *Hydrology and Earth System Sciences*, *10*(6), 873–887. https://doi.org/10.5194/hess-10-873-2006

Kirk, L., & Cohen, M. J. (2022). River corridor sources dominate CO_2 emissions from a lowland river network. *Hydro*. https://doi.org/10.4211/hs.53c0ae4cf09b404fb19a77ed2018e186

Kirk, L., & Cohen, M. J. (2023). River corridor sources dominate CO_2 emissions from a lowland river network. *Journal of Geophysical Research: Biogeosciences*, *128*(1), e2022JG006954. https://doi.org/10.1029/2022JG006954

Koenig, L. E., Helton, A. M., Savoy, P., Bertuzzo, E., Heffernan, J. B., Hall Jr, R. O., & Bernhardt, E. S. (2019). Emergent productivity regimes of river networks. *Limnology and Oceanography Letters*, *4*(5), 173–181. https://doi.org/10.1002/lol2.10115

Leach, J. A., Lidberg, W., Kuglerová, L., Peralta-Tapia, A., Ågren, A., & Laudon, H. (2017). Evaluating topography-based predictions of shallow lateral groundwater discharge zones for a boreal lake-stream system. *Water Resources Research*, *53*(7), 5420–5437. https://doi.org/10.1002/2016WR019804

Maberly, S. C., & Gontero, B. (2017). Ecological imperatives for aquatic CO_2-concentrating mechanisms. *Journal of Experimental Botany*, *68*(14), 3797–3814. https://doi.org/10.1093/jxb/erx201

Mejia, F. H., Fremier, A. K., Benjamin, J. R., Bellmore, J. R., Grimm, A. Z., Watson, G. A., & Newsom, M. (2019). Stream metabolism increases with drainage area and peaks asynchronously across a stream network. *Aquatic Sciences*, *81*(1), 9. https://doi.org/10.1007/s00027-018-0606-z

Mulholland, P. J., Fellows, C. S., Tank, J. L., Grimm, N. B., Webster, J. R., Hamilton, S. K., et al. (2001). Inter-biome comparison of factors controlling stream metabolism. *Freshwater Biology*, *46*(11), 1503–1517. https://doi.org/10.1046/j.1365-2427.2001.00773.x

Odum, H. T. (1956). Primary production in flowing waters. *Limnology & Oceanography*, *1*(2), 102–117. https://doi.org/10.4319/lo.1956.1.2.0102

Raymond, P. A., Zappa, C. J., Butman, D., Bott, T. L., Potter, J., Mulholland, P., et al. (2012). Scaling the gas transfer velocity and hydraulic geometry in streams and small rivers: Gas transfer velocity and hydraulic geometry. *Limnology and Oceanography: Fluids and Environments*, *2*(1), 41–53. https://doi.org/10.1215/21573689-1597669

Regnier, P., Friedlingstein, P., Ciais, P., Mackenzie, F. T., Gruber, N., Janssens, I. A., et al. (2013). Anthropogenic perturbation of the carbon fluxes from land to ocean. *Nature Geoscience*, *6*(8), 597–607. https://doi.org/10.1038/ngeo1830

Reichert, P., Uehlinger, U., & Acuña, V. (2009). Estimating stream metabolism from oxygen concentrations: Effect of spatial heterogeneity. *Journal of Geophysical Research*, *114*(G3). https://doi.org/10.1029/2008JG000917

Rocher-Ros, G., Sponseller, R. A., Lidberg, W., Mörth, C.-M., & Giesler, R. (2019). Landscape process domains drive patterns of CO_2 evasion from river networks. *Limnology and Oceanography Letters*, *4*(4), 87–95. https://doi.org/10.1002/lol2.10108

Rodríguez-Castillo, T., Estévez, E., González-Ferreras, A. M., & Barquín, J. (2019). Estimating ecosystem metabolism to entire river networks. *Ecosystems*, *22*(4), 892–911. https://doi.org/10.1007/s10021-018-0311-8

Segatto, P. L., Battin, T. J., & Bertuzzo, E. (2023). A network-scale modeling framework for stream metabolism, ecosystem efficiency, and their response to climate change. *Water Resources Research*, *59*(3), e2022WR034062. https://doi.org/10.1029/2022WR034062

Shangguan, Q., Lai, C.-Z., Beatty, C. M., Young, F. L., Spaulding, R. S., & DeGrandpre, M. D. (2021). Autonomous in situ measurements of freshwater alkalinity. *Limnology and Oceanography: Methods*, *19*(2), 51–66. https://doi.org/10.1002/lom3.10404

Shangguan, Q., Payn, R. A., Hall, R. O. Jr., Young, F. L., Valett, H. M., & DeGrandpre, M. D. (2024). Divergent metabolism estimates from dissolved oxygen and inorganic carbon: Implications for river carbon cycling. *Limnology & Oceanography*, *69*(9), 2211–2228. https://doi.org/10.1002/lno.12666

Song, C., Dodds, W. K., Trentman, M. T., Rüegg, J., & Ballantyne, F. IV. (2016). Methods of approximation influence aquatic ecosystem metabolism estimates. *Limnology and Oceanography: Methods*, *14*(9), 557–569. https://doi.org/10.1002/lom3.10112

Stan Development Team. (2023). Stan modeling language useres guide and reference manual.

Stets, E. G., Butman, D., McDonald, C. P., Stackpoole, S. M., DeGrandpre, M. D., & Striegl, R. G. (2017). Carbonate buffering and metabolic controls on carbon dioxide in rivers. *Global Biogeochemical Cycles*, *31*(4), 663–677. https://doi.org/10.1002/2016GB005578

Stumm, W., & Morgan, J. J. (2012). *Aquatic chemistry: Chemical equilibria and rates in natural waters* (3rd ed.). John Wiley & Sons, Inc.

Thackston, E. L., & Parker, F. L. (1971). *Effect of geographical location on cooling pond requirements and performance* (Vol. 16130). Environmental Protection Agency, Water Quality Office.

Trentman, M. T., Hall, R. O. Jr., & Valett, H. M. (2023). Exploring the mismatch between the theory and application of photosynthetic quotients in aquatic ecosystems. *Limnology and Oceanography Letters*, *8*(4), 565–579. https://doi.org/10.1002/lol2.10326

Vachon, D., Sadro, S., Bogard, M. J., Lapierre, J.-F., Baulch, H. M., Rusak, J. A., et al. (2020). Paired O_2–CO_2 measurements provide emergent insights into aquatic ecosystem function. *Limnology and Oceanography Letters*, *5*(4), 287–294. https://doi.org/10.1002/lol2.10135

Vrugt, J. A., Ter Braak, C., Diks, C., Robinson, B. A., Hyman, J. M., & Higdon, D. (2009). Accelerating Markov chain Monte Carlo simulation by differential evolution with self-adaptive randomized subspace sampling. *International Journal of Nonlinear Sciences and Numerical Stimulation*, *10*(3), 273–290. https://doi.org/10.1515/IJNSNS.2009.10.3.273

Wanninkhof, R., Asher, W. E., Ho, D. T., Sweeney, C., & McGillis, W. R. (2009). Advances in quantifying air-sea gas exchange and environmental forcing. *Annual Review of Marine Science*, *1*(1), 213–244. https://doi.org/10.1146/annurev.marine.010908.163742

Wolf-Gladrow, D. A., Zeebe, R. E., Klaas, C., Körtzinger, A., & Dickson, A. G. (2007). Total alkalinity: The explicit conservative expression and its application to biogeochemical processes. *Marine Chemistry*, *106*(1), 287–300. https://doi.org/10.1016/j.marchem.2007.01.006